DRC05
The Second TSME International Conference on Mechanical Engineering
October 19-20, 2011, Krabi

Design and Analysis of a Two-Degree of Freedom Cable Driven Compound Joint System

Phongsaen Pitakwatchara

Department of Mechanical Engineering, Faculty of Engineering
Chulalongkorn University, Bangkok, THAILAND 10330
Email: phongsaen.p@chula.ac.th

Abstract

A prototypical two-degree of freedom compound joint system has been designed to imitate the pitch and yaw motion of a human shoulder. Several design criteria are listed. One of them is to achieve the clean motion. Notable cable-pulley power transmission mechanism can provide this desired characteristic and thus has been adopted. It possesses two stages of reduction, with the gear ratio of 3:1 for each of them. Together with the selected D.C. motors, the robot is capable of withstanding the payload of 10 kg at the distance 315 mm from the shoulder center. Due to kinematic constraints, the motion range is limited to $\pm 65°$ for pitch and yaw degree of freedom.

Mathematical model of the system has been developed based on the Euler-Lagrange formulation. In addition, we have employed the bond graph modeling framework to provide the systematic and unified formulation of the equations. Important dynamical effects are taken into account, particularly the compliance and the loss in transmission. This model will be useful for future control and simulation purposes. As a verification of the correctness of the proposed model, two simulations are conducted and their results are discussed.

Keywords*:* shoulder joint, cable-pulley driven robot, flexible joint robot model

1. Introduction

Recent design of robot system has been geared for working synergistically with human, rather than in the well-structured environment as typically seen in the industrial plants. Examples of such famous robotic systems are the Asimo humanoid robot [1], the Care-O-bot service robot [2], the WAM arm [3], and the DLR arm [4]. All have been carefully designed by considering the fundamental dynamics of the system. This results in the simple and natural control law that can realize the desired motion of the robot effectively.

For this project, we aim to develop an anthropomorphic arm which eventually will be equipped to the mobile platform for the service robot. In the beginning phase, we shall focus on designing the shoulder joint that plays a vital role for the whole arm design.

Taking the human arm as a metaphor, we approximate its gross movement, relative to the torso, with eight discrete revolute joints shown in Fig. 1 [5]. Here the shoulder motion is captured by three joints depicted θ_2, θ_3, and θ_4, that are commonly called the pitch, yaw, and roll angle. Several researchers have attempted to devise sophisticated mechanisms to replicate the human shoulder motion, such as the three-DOF cybernetic shoulder that can modify its compliance [6]. The use of parallel mechanism as the shoulder girdle and the serial mechanism to realize the humeral joint results in a complex that mimics the shoulder anatomy closely [7]. However for our purpose as the

prototype supporting the basic study of the cable driven robot, only the pitch and yaw motion (θ_2 and θ_3) are implemented by the developed compound joint.

We use the differential mechanism, which roots from the differential gear train in automobile power transmission, in realizing the two-degree of freedom compound joint. The mechanism transforms the rotational motion of two motors to the rotation of the output linkage about two mutually perpendicular axes. Hence this type of compound joint allows the reproduction of the motion by the ball and socket joint found in the structure of human body. Consequently, it is normally used as the modular joint of advanced robots such as the shoulder joint of the dexterous arm [8], the waist joint of the humanoid robot [9], or the hip, knee, and ankle joint of the biped [10].

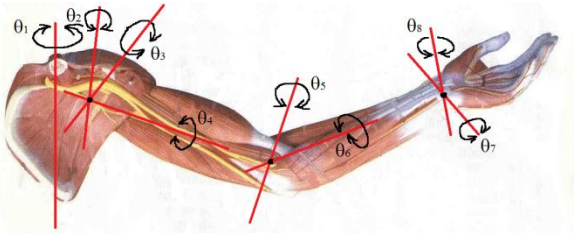

Figure 1: Human arm gross kinematic topology

Rather than achieving the differential mechanism through the gear system, we adopt the cable and pulley system which yields several advantages. If properly designed, the accomplished motion would be cleaner due to lower backlash, noise, and vibration than those occurred in the gearing power transmission system [11]. Also, the simplicity in designing the robot to possess the desired characteristics, such as minimal moving masses by relocating the distal weights to the base, attracts the designer. Furthermore, the inherent compliance of the cable may be employed to improve stability and safety of the robot, especially for the tasks involving the interaction with human and environment.

Organization of the paper is as follow. Section 2 explains the design of our two-degree of freedom compound joint. Key specifications of the system are summarized. Then, in section 3, the analysis of the system is presented of which a dynamical model concerning realistic effects of cable compliance, power loss in transmission, and friction in the bearings is developed. Two simulation results and discussion are given in section 4. Finally we conclude and mention on the future work.

2. Design of the Compound Joint System

In any real-world design, complex decision involving many issues which often are the trade-offs must be conducted. Following is the list of some important design requirements that are taken into consideration. Short descriptions are provided to reflect our thoughts.

2.1 Design Requirements

1. Two-DOF cable driven compound joint: The constructed mechanism is intended to function as the shoulder joint. Its kinematic structure is chosen to be the pitch-yaw arrangement which corresponds to the second and third joint of the arm gross kinematic topology (Fig. 1).
2. High efficiency transmission system: The cable-pulley system is adopted. Attention is paid to the design so it possesses suitable inertial and compliance characteristics.
3. Lightweight system: Since the robot is planned to work cooperatively with human, safety issue must be warranted. Hence the robot should be lightweight as much as possible. However the resulting tendency of deteriorating strength and stiffness of the structure, which in the end will affect its precision and accuracy, curbs this weight reduction process.
4. Counter-balancing mechanism: Another measure for safety criterion, especially when the power is blacked out, is that the robot must be prevented from falling down. The spring-mechanism has been designed to enforce the system status be in near-equilibrium over its workspace. This has another advantage of reducing the size of the motors since the counter-torque has been generated passively.
5. Compact system: To get this robot working in human environment practically without barrier, it must be made compact – like our gifted arm. Due to current technology, we are still far from the line. Furthermore, the use of the cable-pulley power transmission scheme unfortunately makes the system somewhat unwieldy, mainly due to necessarily larger size of pulleys compared to the standard size of gears. This, however, must be reconsidered in the future design of the robot joint and arm.

2.2 Summary of the Mechanism

We have iteratively gone through the design and analysis processes while keeping the above general requirements in mind. A CAD-generated isometric view of the prototype is depicted in Fig. 2. The heart of the mechanism is the use of the cable and pulley systems in implementing the differential mechanism, the reduction

mechanism, as well as the counter-weight balancing mechanism.

Figure 3 illustrates the pulleys' and winches' arrangement of the mechanism and the output upper arm, or shoulder, link. The motor axle is coupled to winch#1 axle, which then drives winch#2 through the wrapped cables. Winch#2 in turn drives pulley#1 (right winch) or pulley#2 (left winch). Altogether with pulley#3, they form the differential mechanism which produces rotational motion of the output linkage about two mutually perpendicular axes. For the specific pose of the shoulder joint, the principal axes of the rotation coincide with the pitch and yaw directions.

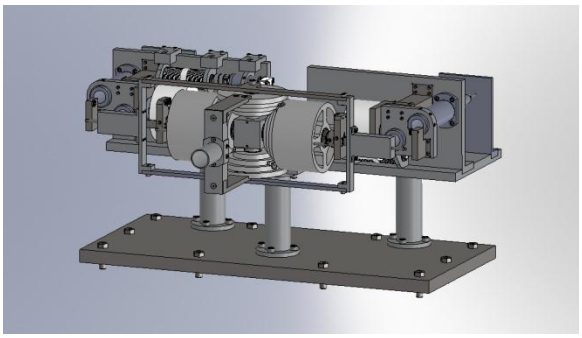

Figure 2: Isometric view of the compound joint

Pulley#4 is not attached with any cable. Its purposes are to counter pulley#3 and strengthen the structure. Pulley#1 to #4 has been shaped into stepped cylinders so the bidirectional power transmission is possible. Diameters of each mating step are equal so the transmission ratio for the pitch and yaw motion are the same. Considering the size limitation and the backdrivability requirement, the ratio of all reduction stages are selected to be 3:1. To help envision the mechanism, its key parameters are listed in Table 1.

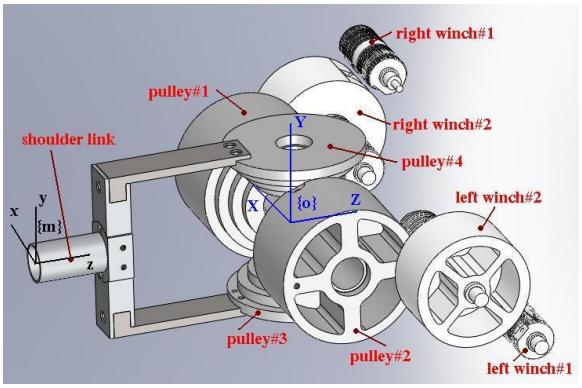

Figure 3: Pulleys' and winches' arrangement

3. Robot Analysis

The goal of this analysis is to develop a dynamical model applicable for the simulation and control purposes. It is based on the important assumption that the cables have been securely wrapped around the pulleys with proper pretension so no slippage between the cable and the pulley's groove. First the kinematics of the mechanism is derived. Next we consider some attributes of the important components, namely the cable compliance, the friction developed between the cable and pulley groove's surface, and the friction loss at the bearing.

Dynamics of the compound joint, including the counterweight, will then be analyzed explicitly. Furthermore, to improve the accuracy of the model, dynamics of the electromechanical parts, specifically the motors, will be taken into account as well. Finally, dynamics of these subsystems and the reduction winches will be combined to achieve the complete model of the robot.

3.1 Kinematics

Let $\dot{\theta}_w$, $\dot{\theta}_1$, $\dot{\theta}_2$, $\dot{\theta}_p$, and $\dot{\theta}_y$ be the angular velocity of the winch, pulley#1, pulley#2, and the pitch and yaw angular velocity component of the shoulder link, respectively. See Fig. 3. Interconnections between these parts by cables and structures pose the following kinematical constraints.

Table 1: Key parameters of the mechanism

Feature	Value
winch#1 diameter	45/135 [mm]
winch#2 diameter	54/162 [mm]
differential pulley diam.	90/114/138/162 [mm]
distal link length	315 [mm]
pitch angle range	$\pm 65°$
yaw angle range	$\pm 65°$
working area	0.37 [m^2]
mass of moving parts	20 [kg]
resolution	0.11 [mm]
max end tip payload	10 [kg]
max end tip velocity	2.6 [m/s]
max end tip acceleration	5.25 [m/s^2]

At the 1st winch-stage

$$\dot{\theta}_{w2r} = \frac{1}{3}\dot{\theta}_{w1r}. \quad (1)$$

$$\dot{\theta}_{w2l} = \frac{1}{3}\dot{\theta}_{w1l}. \quad (2)$$

At the 2nd winch-stage

$$\dot{\theta}_1 = \frac{1}{3}\dot{\theta}_{w2r}. \quad (3)$$

$$\dot{\theta}_2 = \tfrac{1}{3}\dot{\theta}_{w2l}. \quad (4)$$

At the differential mechanism

$$\dot{\theta}_p = 0.5(\dot{\theta}_1 + \dot{\theta}_2). \quad (5)$$

$$\dot{\theta}_y = 0.5(\dot{\theta}_1 - \dot{\theta}_2). \quad (6)$$

Hence the velocity at the end point of the output link may be determined simply from the fact that the link motion is the pure rotation about the origin of fixed $\{XYZ\}$. In other words,

$${}^m\bar{v}_e = ({}^m\bar{\omega}_p + {}^m\bar{\omega}_y) \times {}^m\bar{r}_e,$$

where its angular velocity is decomposed along the pitch and yaw directions, denoted as ${}^m\bar{\omega}_p$ and ${}^m\bar{\omega}_y$. ${}^m\bar{r}_e = {}^m[0 \quad 0 \quad -l_o]^T$ is the position vector of the end point with $l_o = 315$ mm for the current design. All quantities are expressed in the moving $\{xyz\}$ attached to the output link at the end point. Completing the evaluation, the end point velocity is

$${}^m\bar{v}_e = {}^m\begin{bmatrix} -l_o\dot{\theta}_y & l_o\dot{\theta}_p c_y & 0 \end{bmatrix}^T, \quad (7)$$

where in this paper we abbreviate, for example, s_y and c_y for $\sin\theta_y$ and $\cos\theta_y$ respectively.

Relative rotation between $\{xyz\}$ and $\{XYZ\}$ is captured by the rotation matrix

$${}^oR_m = \begin{bmatrix} c_y & 0 & s_y \\ s_p s_y & c_p & -s_p c_y \\ -c_p s_y & s_p & c_p c_y \end{bmatrix}. \quad (8)$$

It may be used to express the end point velocity in the fixed $\{XYZ\}$:

$${}^o\bar{v}_e = {}^o\begin{bmatrix} -l_0\dot{\theta}_y c_y \\ l_0\dot{\theta}_p c_p c_y - l_0\dot{\theta}_y s_p s_y \\ l_0\dot{\theta}_p s_p c_y + l_0\dot{\theta}_y c_p s_y \end{bmatrix}, \quad (9)$$

which is helpful for tracking control purpose. From this expression and Eqs. (1)-(6), the Jacobian matrix mapping the angular velocity of the input motors to the end point velocity may be deduced directly as

$${}^oJ = {}^o\begin{bmatrix} \frac{-l_0 c_y}{18} & \frac{l_0 c_y}{18} \\ \frac{l_0 c_p c_y - l_0 s_p s_y}{18} & \frac{l_0 c_p c_y + l_0 s_p s_y}{18} \\ \frac{l_0 s_p c_y + l_0 c_p s_y}{18} & \frac{l_0 s_p c_y - l_0 c_p s_y}{18} \end{bmatrix}. \quad (10)$$

3.2 Compliance and Efficiency of the Cable-Pulley Power Transmission System

Compliance characteristic of the simple cable-pulley drive unit was developed in [12]. The result will now be extended for the case of the differential cable-pulley mechanism. Consider the simplified diagram of the mechanism in Fig. 4 where pulley#3 is driven by pulley#1 and pulley#2. A half cable circuit is shown.

First, the rotational stiffness about the pitch axis will be determined. Assume the related cables are pretensioned to the value of T_o. Then, both the driving pulley#1 and #2 are securely fixed. Next, external moment $\bar{M}_p$ along the pitch axis is applied to pulley#3. We would like to determine the associated deflected angle θ_p. The derivation applies the constitutive relation of the change in the cable tension and the elongation to the geometric and equilibrium constraints of the cable-pulley system. Details are given in [13].

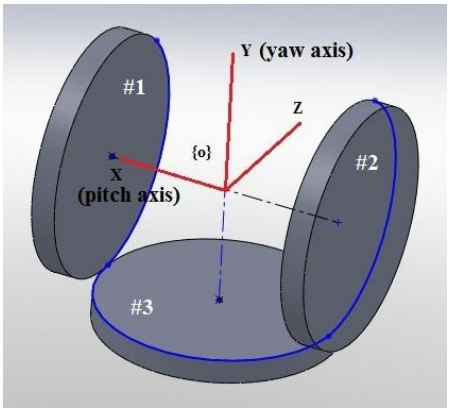

Figure 4: Simplified diagram of the differential mechanism

When the ratio of the unwrapped cable length, L, to the radius of the wrapped pulley, R, is negligible, the equations for the equilibrium tensions and the deflected angle subject to the applied moment may be obtained explicitly. As a result, the rotational stiffness of the differential cable-pulley mechanism about the pitch axis, K_p, becomes

$$K_p = 2EA\mu_{\text{eff}}\frac{R_1^2}{R_3}\left(\frac{\left(e^{m/2}-1\right)^2}{e^{m/2}\left(e^{m/2}-\frac{m}{2}-1\right)}\right) \times \left(1 + GF - \frac{e^{m/2}-1}{me^{m/2}/2}\right)^{-1}, \quad (11)$$

where E and A are the Young modulus and the cross sectional area of the cable. μ_{eff} the dynamic coefficient of friction between the cable and the pulley's groove. Radius of the pulley#1 and #3 are R_1 and R_3. $m = M_p/T_o R_1$ is the dimensionless moment and $GF = L\mu/R_3$ is the geometric friction number that dictates the compliance response behavior.

Similar derivation may be performed to obtain the rotational stiffness about the yaw axis, K_y, as

$$K_y = 2EA\mu_{\text{eff}}R_3\left(\frac{\left(e^{m/2}-1\right)^2}{e^{m/2}\left(e^{m/2}-\frac{m}{2}-1\right)}\right) \times \left(1 + GF - \frac{e^{m/2}-1}{me^{m/2}/2}\right)^{-1}, \quad (12)$$

while in this case the dimensionless moment is calculated from the applied moment $\bar{M}_y$ along the yaw axis as $m = M_y/T_o R_3$. As the applied moment approaches zero, the stiffness values converge to

$$K_p = \frac{4EAR_1^2}{L}, \tag{13}$$

and

$$K_y = \frac{4EAR_3^2}{L}. \tag{14}$$

Variation of the cable tension along the length causes any segment to undergo elongation and contraction in a cyclic manner. Therefore, when the pulleys are rotating in dynamic equilibrium, cable slippage will occur at the groove of the wrapped pulley. Developing friction will then do the resistive work, resulting in the lost power. Consequently, we may model the friction indirectly via the efficiency of the power transmission.

The transmission efficiency of the simple cable-pulley drive unit was developed in [12]. Its result will now be extended for the case of the differential cable-pulley mechanism. Lost power, P_l, may be determined by summing the infinitesimal power generated by the friction force over the wrapped portion. The infinitesimal power is calculated by multiplying the friction force, $F_{\text{fr}}(\theta)$, with the time rate of change of the cable stretch/contraction, $\delta(\theta)$, at that point. That is,

$$dP_l(\theta) = F_{\text{fr}}(\theta)\frac{d\delta(\theta)}{dt}.$$

Integrating the infinitesimal power for the entire wrapping range (noting that the output pulley#3 is wrapped with double-loop circuit), the power loss becomes

$$P_{li} = \frac{P}{2}\frac{T_h - T_l}{2EA}, \tag{15}$$

and

$$P_{lo} = P\frac{T_h - T_l}{2EA}, \tag{16}$$

for the input and output pulley, respectively. P is the power supplied to the output pulley of radius R by the applied moment M that may be determined from $P = M\omega = 2\omega R(T_h - T_l)$. Power to each input pulley will be half of it, i.e. $\frac{P}{2}$.

The power two input pulleys delivered to the cables must equal the power the output pulley took from the cable. This fact may be written as

$$P_{\text{in}}\left(1 - \frac{T_h - T_l}{2EA}\right) = P_{\text{out}}\left(1 + \frac{T_h - T_l}{2EA}\right),$$

where P_{in} represents the total supplied power to the input pulleys and P_{out} the output power from the mechanism. Therefore the transmission efficiency, $\eta = \frac{P_{\text{out}}}{P_{\text{in}}}$, may be determined;

$$\eta = 1 - \frac{M}{2REA}, \tag{17}$$

under the assumption $\frac{T_h - T_l}{2EA} \ll 1$.

3.3 Friction Loss at the Bearing

From the estimated calculation, friction loss at the bearing is of the same order, or even larger, than the loss at the cable-pulley transmission system. Model complexity prevents one to search for the theoretical equations. Rather, the *conservative* empirical formulation of the frictional torque for the standard sealed deep-groove ball bearing [15]

$$M_{\text{fr}} = 35812.5\frac{Hd}{nr}, \tag{18}$$

will be used to approximate the actual friction at each unsealed angular contact ball bearing. In the formula, M_{fr} [Nmm] is the friction torque, d [mm] the shaft diameter, r [mm] the pulley radius, n [rad/s] the angular velocity of the pulley, and H [kW] the transmitted power.

3.4 Dynamics of the Compound Joint

Compound joint mainly consists of pulley#3, pulley#4, and the output link. These components have complicated motion subject to the primitive pitch and yaw motion. Therefore, the Euler-Lagrange formulation is adopted to account for deriving its equations of motion. As a matter of convenience, the counterweight mechanism subject to the pitch motion solely will be included.

Only outline of the derivation will be given here. The details are reported in [13]. First, for the sake of visualization, the mechanical parts are grouped into two aggregates: one under the pitching motion only and the other under the composite pitching and yawing motion. Next, with the help of kinematics analysis, the associated kinetic and potential energies may be expressed in terms of generalized coordinates and velocities.

After that, formulating the equations of motion is rather straightforward. Lagrangian for this subsystem

$$\mathcal{L} = T_p + T_{py}$$

is formed from the kinetic energy of both aggregates. Potential energy is handled exclusively for the purpose of distinct gravity torques (gradient of the potential energy) and the design of the compensator. According to two generalized coordinates for this compound joint, namely θ_p and θ_y, the Euler-Lagrange formulation for this holonomic system becomes

$$\frac{d}{dt}\left(\frac{\partial \mathcal{L}}{\partial \dot{\theta}_p}\right) - \frac{\partial \mathcal{L}}{\partial \theta_p} = \tau_p,$$

and

$$\frac{d}{dt}\left(\frac{\partial \mathcal{L}}{\partial \dot{\theta}_y}\right) - \frac{\partial \mathcal{L}}{\partial \theta_y} = \tau_y.$$

τ_p and τ_y are the corresponding generalized torques. Substituting the Lagrangian into the above formulations, the

equations of motion arranged in the standard form are determined. The expressions are quite unwieldy and so shall be excluded.

3.5 Motor Dynamics

Motor may be viewed as the instrument which transforms the electrical power into the mechanical power. Hence it is natural to employ the bond graph modeling framework in developing the consistent governing equations. To improve the model accuracy, we have included the inertia effects and losses in both domains. As a result, the bond graph model of a DC permanent magnet motor may be drawn as shown in Fig. 5. GY is the motor torque constant, I_i the inductance of the armature coil, I_m the rotor inertia, R_i the coil resistance, and S_e the gross mechanical friction in the support.

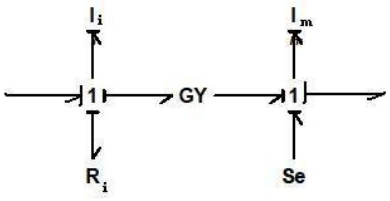

Figure 5: Bond graph model of
a DC permanent magnet motor

3.6 Complete Model

Dynamics of the reduction winches can be determined readily because they are constrained to be rotating about the fixed axes. The governing equation is simply

$$\tau_i = I_{ii}\ddot{\theta}_i,$$

where all quantities are taken about the rotation axis i. Compliance and efficiency of the pertaining cable circuits are derived in [12][14].

All of these components are physically assembled to be a cable driven compound joint system. In analogy, equations of motion of each subsystem must be integrated to form a complete model of the system. We apply the bond graph modeling framework to incorporate these equations systematically in a unified manner. Briefly, all important dynamical effects of every subsystem, namely the power transformation (TF, GY), the inertia (I), the compliance (C), and the loss (R, S_e) of motors, winches, pulleys, bearings, cables, springs, and linkages are combined to form the complete model of the system. Graphical bond graph model showing the overall structure and the interconnection are depicted in Fig. 6. The system equations of motion may be determined directly from the diagram.

4. Simulation

The developed model will now be used to simulate the robot's free motion. This is purposely to validate, to a certain extent, the correctness of our model. The system is set up to start off from rest at the middle point of the workspace. At this posture, the distal link points in the opposite direction to the reference horizontal Z-axis as illustrated in Fig. 3.

Since the system is not powered, the link is expected to fall down due to the gravity. However, from the simulation result plotted in Fig. 7, we see that the output link gradually pitches up and eventually stops at the upright posture. This is due to the equipped spring-counterweight mechanism. It has been intentionally designed such that it is capable of providing the counter-gravity torque perfectly. Therefore, the ideal system would be in static equilibrium at arbitrary posture. Unfortunately, the standard tension springs available have some degrees of nonlinearity. Particularly, the initial tension is nonzero. This produces the mismatch in the required spring force and hence the counter-gravity torque.

From this characteristic, the equilibrium of the system may then be determined by searching for the set of generalized coordinates which satisfy zero gradient of the total potential energy equation. Consequently, the equilibrium points are contained in the set

$$E = \left\{\bar{X} \middle| \theta_p + \theta_y = \frac{\pi}{2}, x_i = 0\right\}, \quad (19)$$

for which $\bar{X}$ is the state vector of the system. In other words, at the equilibrium point, all state variables will be zero except the pitch and yaw angles, of which their values must sum to $90°$.

The second simulation is conducted where the system is initially at rest with the distal link at the posture where the pitch angle still be $0°$ but the yaw angle set to $20°$. Figure 8 shows the free response of the output link. The states asymptotically approach an equilibrium point satisfying E; in this case $\theta_{p*} = 65°$ and $\theta_{y*} = 25°$.

5. Conclusions and Future Work

A prototypical two-degree of freedom cable driven compound joint system, serving as the shoulder part of the service robot arm, has been designed. Some parameters and performance indices are given. Furthermore, important

characteristics, such as the compliance and the loss in cable-pulley transmission, of the system have been analyzed upon which the detailed model is developed. The system is simulated and the result is examined. It agrees with the equilibrium analysis.

We plan to construct the designed prototype to investigate its actual behavior. Subsequently the model will be corrected, improved, and validated. Comprehension in the model itself will be used to develop suitable controller. We expect the knowledge base from experimenting with this prototype will be helpful in the design and control of the cable-driven robotic systems.

6. Acknowledgements

The author would like to express his gratitude to Prof. Viboon Sangveraphunsiri for fruitful criticism and financial support. Grants from the Research Promoting Fund of Faculty of Engineering, the New Faculty Initiative Fund of the Department of Mechanical Engineering, and the ISUZU Foundation are cordially appreciated.

7. References

[1] Sakagami, Y., et al. (2002). "The Intelligent ASIMO: System Overview and Integration," *Proc. IROS*, pp. 2478-2483.

[2] Graf, B., et al. (2004). "Care-O-bot II–Development of a Next Generation Robotic Home Assistant," *Autonomous Robots*, Vol. 16, pp. 193-205.

[3] Rooks, B. (2006). "The Harmonious Robot," *Int. J. Industrial Robot*, Vol. 33, No. 2, pp. 125-130.

[4] Albu-Schaffer, A., et al. (2007). "The DLR Lightweight Robot – Design and Control Concepts for Robots in Human Environments," *Int. J. Industrial Robot*, Vol. 34, No. 5, pp. 376-385.

[5] Modified of picture taken from Human AnatomyLaboratory, University of Colorado, URL: http://www.colorado.edu/intphys/iphy3415/resources.html accessed on May 30th, 2011.

[6] Okada, M. and Nakamura, Y. (2005). "Development of a Cybernetic Shoulder – A Three-DOF Mechanism that Imitates Biological Shoulder Motion," *IEEE Trans. Robotics*, Vol. 21, No. 3, pp. 438-443.

[7] Lenarcic, J. and Stanisic, M. (2003). "A Humanoid Shoulder Complex and the Humeral Pointing Kinematics," *IEEE Trans. Robotics and Automation*, Vol. 19, No. 3, pp. 499-506.

[8] Townsend, W. (1988). "The Effect of Transmission Design on Force-Controlled Manipulator Performance," *Ph.D. Dissertation*, MIT.

[9] Hinojosa, W. M., et al. (2006). "Performance Assessment of a 3 DOF Differential Based Waist Joint for the 'iCub' Baby Humanoid Robot," *IEEE Int. Symp. Robot and Human Interactive Communication (RO-MAN)*, pp. 195-201.

[10] Olaru, I. M. C., et al. (2009). "Novel Mechanism Design of Biped Robot SHERPA Using 2 DOF Cable Differential Modular Joints," *IEEE/RSJ Int. Conf. Intelligent Robots and Systems (IROS)*, pp. 4463-4468.

[11] Schempf, H. (1990). "Comparative Design, Modeling, and Control Analysis of Robotic Transmission," *Ph.D. Dissertation*, MIT.

[12] Snow, E. R. (1993). "The Load/Deflection Behavior of Pretensioned Cable/Pulley Transmission Mechanisms," *M.S. Thesis*, MIT.

[13] Pitakwatchara, P. (2011). "A Two-Degree of Freedom Cable Driven Compound Joint System," *Internal Report to the Research Promoting Fund of Faculty of Engineering,* Chulalongkorn University Robotics Laboratory (CURL).

[14] Pitakwatchara, P. (2010). "Analysis and Modeling of the Cable-Pulley Power Transmission System in Robot," *Proc. IASTED Int. Conf. Robotics (ROBO)*, pp. 136-140.

[15] Nippon System Kaihatsu (2007). "NSK Rolling Bearing Catalog," CAT. No. E1102e.

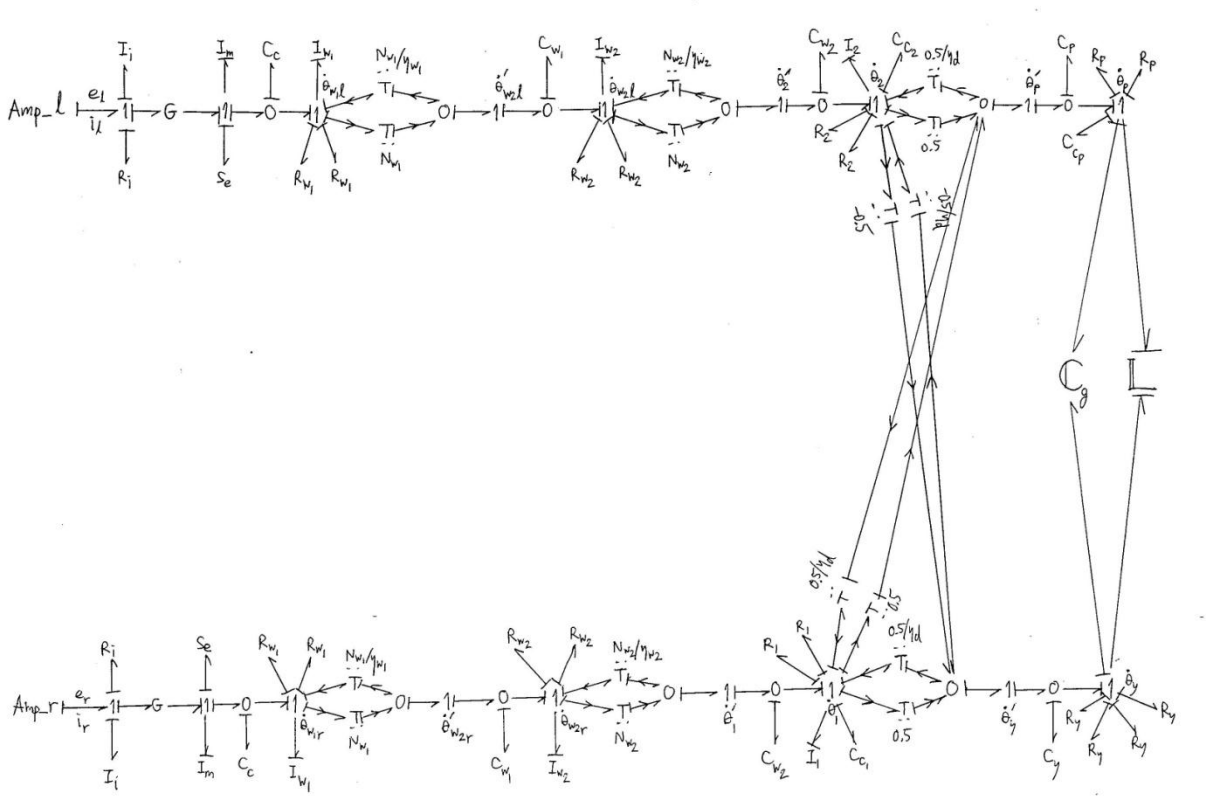

Figure 6: Bond graph model of the two-degree of freedom compound joint system

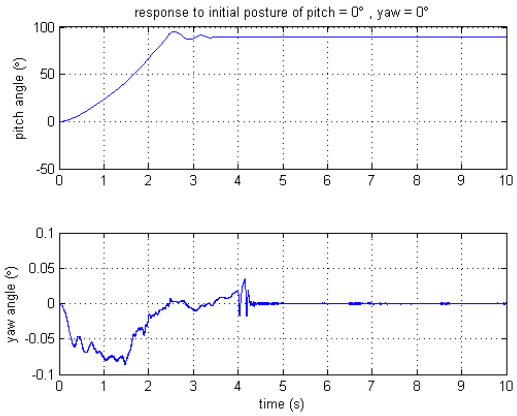

Figure 7: Response of the pitch and yaw motion of the output link with initial values of $(0°, 0°)$

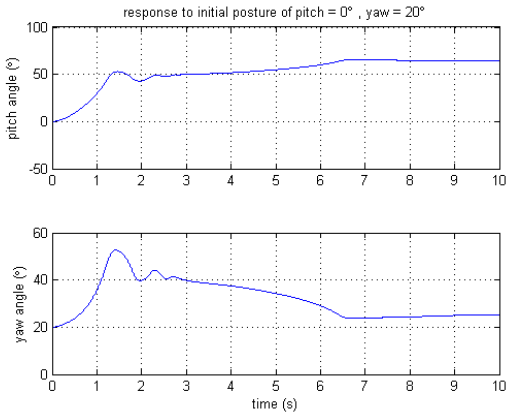

Figure 8: Response of the pitch and yaw motion of the output link with initial values of $(0°, 20°)$